MEASUREMENTS AND STUDIES ON THE NONLINEAR DISPERSION IN THE ESR

A. Sherjan*[1,2], G. Franchetti[1,2,3], J. Rausch[2], B. Lorentz[1]
[1]GSI Helmholtz Centre for Heavy Ion Research, Darmstadt, Germany
[2]Goethe University Frankfurt, Frankfurt am Main, Germany
[3]HFHF Helmholtz Research Academy Hesse for FAIR, Frankfurt am Main, Germany

Abstract

The ESR storage ring at GSI provides a variety of highly charged heavy ion beams over a wide range of β_{rel} from 85% down to 10% to carry out atomic physics experiments. According to experimental requirements the beam can be either stored and accumulated or decelerated. However, over the whole process of deceleration the beam intensity reduces by a significant factor, while at the same time the beam performs enormous closed orbit (CO) swings at the location of certain beam position monitors (BPMs). From the measured CO, the evolution of $\delta p/p$ during deceleration can be determined and applied on the cycle to compensate the CO swing. This procedure should allow retrieving identical $\delta p/p$ evolution at each BPM. However, the reconstructed $\delta p/p$ from the measurements shows an inconsistency between different BPMs. Therefore the correction procedure cannot be applied and a precise knowledge on the dispersion is required. On this ground the ESR dispersion was measured and the presence of high order terms could be identified. We here present the nonlinear dispersion measurements and discuss potential sources based on simulations.

MOTIVATION

During the Machine Development (MD) 2024 at the ESR, see for reference [1], first measurements were taken to characterize the beam losses during deceleration. There the CO was measured from injection to extraction with 12 BPMs along the ring. In parallel, also the beam intensity was stored with a DC current transformer. As shown in the mid-section of Fig. 1, the beam performs large CO swings during deceleration at the position of the BPMs. In the top-section of Fig. 1 the normalized relative change of the beam intensity highlights simultaneous peaks of beam losses. The CO swings indicate an asynchronization between the cavity frequency and the magnet ramp, which results in an additional dispersive term with a coherent time dependent $\delta p/p$. Therefore the CO swing during deceleration, $X_{CO,j,meas}$, at each BPM, $j = 1, \ldots, 12$, can be described as the sum of the initial CO distortion during storage, $X_{0,j}$, and the dispersive component, $D_{x,j} \cdot \frac{\delta p}{p}(t)$ [2]:

$$X_{CO,j,meas}(t) = X_{0,j} + D_{x,j} \cdot \frac{\delta p}{p}(t) \; . \qquad (1)$$

Consequently, the CO swings can be compensated by determining the evolution of $\delta p/p$ during the ramp and applying it as a correction on the cavity. By subtracting from each CO swing its initial CO distortion, the resulting curves should only differ from one BPM to another by a constant "scaling" factor, $f_j = D_{x,i}/D_{x,j}$, if we assume that the dispersion is not changing during the deceleration. Here the index i is a reference BPM arbitrarily chosen, which is taken fix for all BPMs. Therefore, the quantity

$$X_{CO,j,mod}(t) = [X_{CO,j,meas}(t) - X_{0,j}]f_j = D_{x,i}\frac{\delta p}{p}(t) \qquad (2)$$

should be the same function for all BPMs. Bottom section of Fig. 1 shows the $X_{CO,j,mod}$ for all BPMs, and we clearly see two distinct groups of curves. This implies that the dispersion might also change during deceleration, specifically in two ways according to its position in the ring. With these findings the time evolution of $\delta p/p$ cannot be determined in a unique way. Resolving this discrepancy requires first a more accurate description of the present machine and its optical functions, especially of the dispersion. Therefore, in the MD 2025 a major focus on beam optics to improve the lattice model [3] has been undertaken.

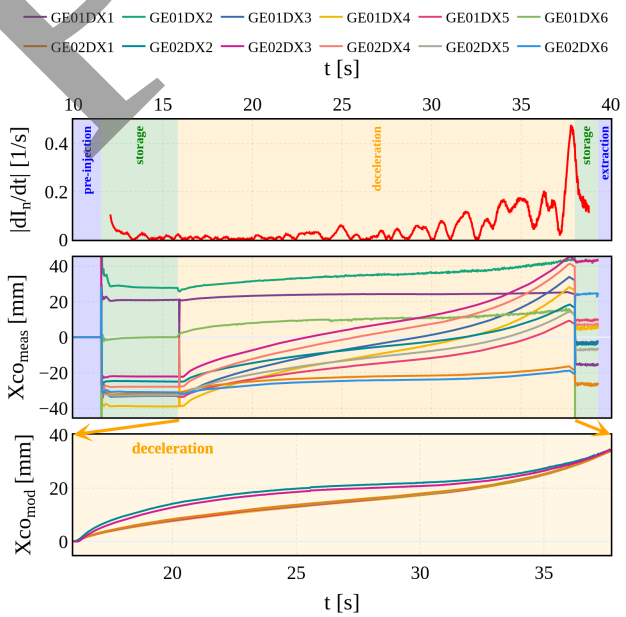

Figure 1: Top: Measurement of the normalized beam intensity deviation shows critical moments during the cycle. Center: At the same time the CO was also stored at the position of the 12 BPMs in the ring. Bottom: CO during deceleration after applying Eq. (2).

* a.sherjan@gsi.de

Preprint

MEASUREMENT

At injection energy the CO of the beam was stored for several $\delta p/p$ by changing the cavity frequency. Using Eq. (1), the dispersion is therefore obtained with the difference in CO divided by the difference in $\delta p/p$ of two measurements, which in case of nonlinearities can be composed of higher-order terms:

$$D_{x,i} = \frac{\Delta X_{CO,meas}}{\Delta (\delta p/p)} = D_{x,i(0)} + D_{x,i(1)} \frac{\delta p}{p} + D_{x,i(2)} \left(\frac{\delta p}{p}\right)^2 + \dots \quad (3)$$

On the top plot of Fig. 2 each curve represents the dispersion at the position of one BPM in the ring. As this plot shows, the dispersion changes nonlinearly depending on $\delta p/p$. A polynomial fit can be applied to obtain the first few orders of the nonlinear dispersion. On the bottom plot of Fig. 2 the zero

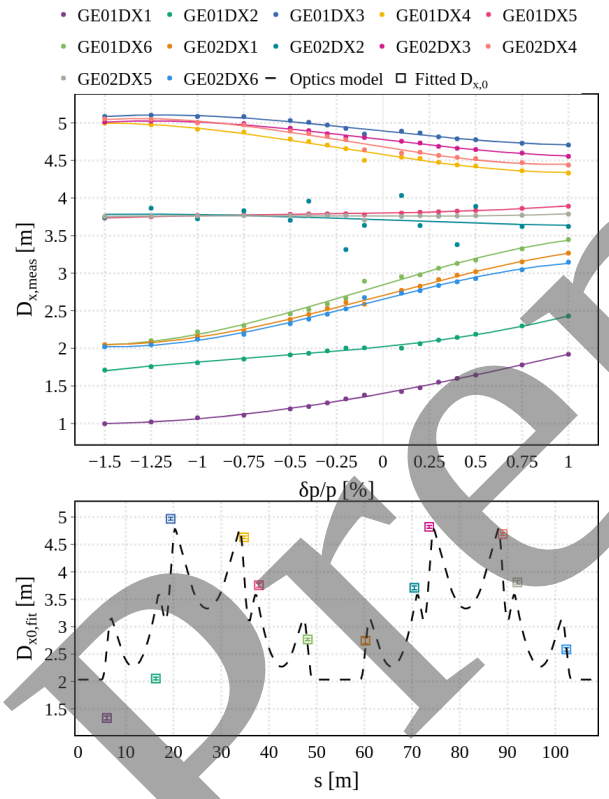

Figure 2: Top: Measurement of the nonlinear dispersion. Bottom: Simulated dispersion from optics model and zero order dispersion from polynomial fit.

order dispersion from the polynomial fit is depicted alongside the dispersion from the theoretical optics model. Note that the measured dispersion at the first two BPM breaks the ESR symmetry, since they are much off compared to the rest, but its origin is not understood. Apart from the measurements of these two BPMs, the nonlinear behavior of the dispersion can be divided in three groups. These three groups are seemingly converging for larger negative $\delta p/p$ values and split towards larger positive $\delta p/p$.

ERROR ANALYSIS

Some measurement values were repeated three times, so that they can be used to estimate the precision of the measurements at each BPM and to analyse its impact on the polynomial fit to retrieve the higher-order dispersion terms. Therefore the standard deviation, σ_{meas}, at each BPM can be determined using the three measurement points. Here the σ_{meas} fluctuates from one BPM to another between 2.3×10^{-3} mm and 4.5×10^{-2} mm. Then for each BPM the σ_{meas} was assumed as the sigma range for each data point of the polynomial fit. Table 1 shows the first few orders of the dispersion with their uncertainties, taking σ_{meas} into account.

Table 1: Approximated Higher-Order Components of the Dispersion Listed for each BPM Together with the Fitting Uncertainties Originating from the Measurement Precision

BPM	$D_{x,(0)}$ [m]	$D_{x,(1)}$ [m]	$D_{x,(2)}$ [m]
GE01DX1	$1.4 \pm 1 \times 10^{-5}$	$44.9 \pm 2 \times 10^{-3}$	$928 \pm 2 \times 10^{-1}$
GE01DX2	$2.0 \pm 1 \times 10^{-6}$	$25.7 \pm 1 \times 10^{-3}$	$1039 \pm 1 \times 10^{-1}$
GE01DX3	$4.9 \pm 3 \times 10^{-6}$	$-26.1 \pm 8 \times 10^{-4}$	$117 \pm 7 \times 10^{-2}$
GE01DX4	$4.6 \pm 2 \times 10^{-6}$	$-37.8 \pm 5 \times 10^{-4}$	$612 \pm 4 \times 10^{-2}$
GE01DX5	$3.8 \pm 8 \times 10^{-7}$	$4.41 \pm 2 \times 10^{-4}$	$320 \pm 2 \times 10^{-2}$
GE01DX6	$2.8 \pm 3 \times 10^{-6}$	$74.6 \pm 6 \times 10^{-4}$	$-382 \pm 5 \times 10^{-2}$
GE02DX1	$2.7 \pm 1 \times 10^{-5}$	$65.7 \pm 3 \times 10^{-3}$	$-4.14 \pm 3 \times 10^{-1}$
GE02DX2	$3.7 \pm 2 \times 10^{-5}$	$-9.15 \pm 3 \times 10^{-3}$	$19.9 \pm 3 \times 10^{-1}$
GE02DX3	$4.8 \pm 8 \times 10^{-6}$	$-29.3 \pm 2 \times 10^{-3}$	$83.4 \pm 2 \times 10^{-1}$
GE02DX4	$4.7 \pm 1 \times 10^{-6}$	$-39.6 \pm 3 \times 10^{-4}$	$621 \pm 2 \times 10^{-2}$
GE02DX5	$3.8 \pm 2 \times 10^{-6}$	$-0.56 \pm 5 \times 10^{-4}$	$215 \pm 4 \times 10^{-2}$
GE02DX6	$2.7 \pm 8 \times 10^{-7}$	$63.1 \pm 2 \times 10^{-4}$	$-377 \pm 2 \times 10^{-2}$

As shown in this table, the uncertainties of the determined dispersion components are relatively very small compared to the actual polynomial coefficients. Therefore the next step is to take these higher-order dispersion values for each BPM as a reference for the dispersion simulations.

SIMULATION

In the following the simulated dispersion will be discussed qualitatively introducing more complexity into the optics model to assess potential sources of the measured nonlinear dispersion in the ESR. The simulations can be compared with the measurement results in Fig. 3a. As a first approach the dispersion was simulated with the same settings for the quadrupole and sextupole magnets as in the measurement, assuming no further perturbations of the initial lattice, see Fig. 3b. The initial lattice also incorporates the correction factors for the quadrupole strengths as suggested from the measurements for the beam based optimization of the linear optics model [3], which were performed likewise the dispersion measurements in the same measurement campaign. From this first case, we can conclude that the formation of the three nonlinear dispersion groups is already visible in the bare lattice configuration, so it is related to the ESR symmetry and the presence of the sextupole magnets. Also the covered dispersion range is roughly the same. But the underlying nonlinear relation is very different and requires further adjustment of the lattice. In the next step the effects of small perturbations added only to the quadrupole magnet strengths are tested. Therefore all the quadrupoles in the lattice are grouped in families of four due to the ESR symmetry and to

Preprint

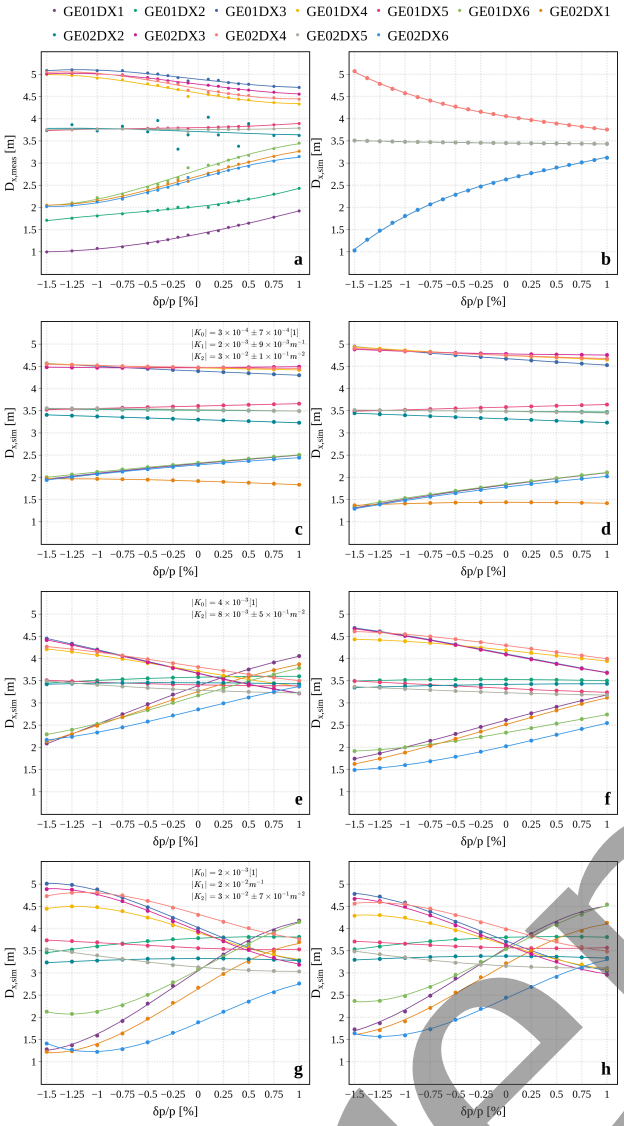

Figure 3: a) Measurement of the nonlinear dispersion. b) Simulation using bare lattice. Note: All curves overlap perfectly into three groups. c) Small perturbation of quadrupoles. d) Additional change of machine tune by $\Delta Q_x = +0.02$. e) Small pertubation of sextupoles. f) Additional change of machine tune by $\Delta Q_x = +0.05$. g) Combination of quadrupole and sextupole perturbation. h) Additional change of machine tune by $\Delta Q_x = -0.02$.

each family a different set of small multipolar kicks, of zero to second order (of strength $|K_0|, |K_1|, |K_2|$ see in Fig. 3c), are added. The simulated dispersion in this case is shown in Fig. 3c. Compared to the bare lattice this configuration maintains the three groups, while it also creates a splitting within each group as it happens in the measurements. The nonlinear trend is only roughly similar to the measurements, as the optics seems not sensitive to small deviations around this setting. The zero order perturbation (of strength $|K_0|$ see in Fig. 3c) implemented in one of the quadrupole families is also used as a knob to move the point of convergence of the three groups along $\delta p/p$. Figure 3d shows how changing the machine tune by $\Delta Q_x = +0.02$ pushes the three groups apart while preserving all the other properties. Next step is to check the impact of small perturbations on the sextupole magnets. One observation is presented in Fig. 3e, where only second order perturbations (of strength $|K_2|$ see in Fig. 3e) are implemented into the sextupoles, which assumes a small deviation of the sextupole strength, to test the dependency of the nonlinear dispersion shape on the sextupole components. Here the splitting and nonlinear shape of the three groups are more pronounced. Also here, an additional knob (of strength $|K_0|$ see in Fig. 3e) was implemented to move the convergence point of the groups. And in Fig. 3f in analogy to the quadrupole case before, the machine tune was changed now by $\Delta Q_x = +0.05$, which again leads to a widening of the three groups. Lastly, a combination of sextupole and quadrupole perturbations (of strength $|K_0|, |K_1|, |K_2|$ see in Fig. 3g) was also tested and is presented in Fig. 3g, where additionally to the sextupoles, as described above, also one quadrupole was given a small quadrupolar deviation. This mixed configuration allows to modify the nonlinear shape of the dispersion, which becomes more similar to the measurements apart from the larger splitting of each group. From Fig. 3g to Fig. 3h the machine tune was changed by $\Delta Q_x = -0.02$, which corresponds to a more narrow distribution of the three groups. The simulations show that several parameters can create and shape the nonlinear dispersion, with small perturbations in the magnets being one possible cause. Therefore the knowledge about the high order multipoles of the ESR magnets is necessary to improve the optics model, which also benefits related measurements and studies on the resonance crossing in the ESR [4].

CONCLUSION

The dispersion measurements at the ESR have revealed the existence of higher-order components. The robustness of the polynomial coefficients was discussed considering possible fluctuations of repeated measurements. A series of simulations with greater detail of the original lattice was tested and indicates a combination of different sources for the nonlinear dispersion, which with all the possible variations adds a lot of complexity. Therefore the discrepancy between the simulation and the measurement can not yet be fully resolved as it requires the knowledge about the exact properties of all the magnets. Consequently beam based measurements to obtain more accurate machine and magnet properties will be necessary in the future. A more precise model would also allow to describe the impact of the additional higher-order components of the dispersion on the momentum compaction, which is relevant for the operation of the storage ring in the isochronous mode [5] and for the deformation of the deceleration bucket.

ACKNOWLEDGEMENTS

The authors would like to thank the ESR operation team for preparing the ESR machine for the measurements and Oleksandr Chorniy for the support on the beam diagnostics.

Preprint

REFERENCES

[1] B. Franzke, "The heavy ion storage and cooler ring project ESR at GSI," *Nucl. Instrum. Methods Phys. Res. B*, vol. 24–25, pp. 18–25, 1987. doi:10.1016/0168-583X(87)90583-0

[2] K. Wille, "The Physics of Particle Accelerators: An Introduction," Oxford University Press, 2000. ISBN: 0-19-850550-7.

[3] A. Heinz, G. Franchetti, A. Sherjan, J. Rausch and B. Lorentz, "Beam based optimization of the ESR linear optics model", presented at IPAC'26, Deauville, France, May 2026, paper WEP5015, this conference.

[4] A. Sherjan, G. Franchetti and J. Rausch, "Experimental Resonance studies at the ESR", presented at IPAC'26, Deauville, France, May 2026, paper THP4075, this conference.

[5] S.A. Litvinov, R. Hess, B. Lorentz, and M. Steck, "Isochronous Mode of the Experimental Storage Ring (ESR) at GSI", in *Proc. IPAC'22*, Bangkok, Thailand, Jun. 2022, pp. 1620–1623. doi:10.18429/JACoW-IPAC2022-WEOYGD3

Preprint